Extended partial-wave analysis of πN scattering data

R. A. Arndt, W. J. Briscoe, I. I. Strakovsky, and R. L. Workman
Center for Nuclear Studies, Department of Physics, The George Washington University, Washington, DC 20052, USA
(Received 7 June 2006; published 23 October 2006)

We present results from a comprehensive partial-wave analysis of $\pi^{\pm}p$ elastic scattering and charge-exchange data, covering the region from threshold to 2.6 GeV in the lab pion kinetic energy, employing a coupled-channel formalism to simultaneously fit $\pi^- p \to \eta n$ data to 0.8 GeV. Our main result, solution SP06, utilizes a complete set of forward and fixed-t dispersion relation constraints applied to the πN elastic amplitude. The results of these analyses are compared with previous solutions in terms of their resonance spectra and preferred values for couplings and low-energy parameters.

DOI: 10.1103/PhysRevC.74.045205 PACS number(s): 14.20.Gk, 13.30.Eg, 13.75.Gx, 11.80.Et

I. INTRODUCTION

Most N and Δ resonances, listed as 3- and 4-star states in the Review of Particle Properties (RPP) [1], have had their existence, masses, and widths determined through single-channel fits to scattering data, with πN elastic scattering being the predominant source. The most comprehensive πN analyses have been performed by the Karlsruhe-Helsinki (KH) [2], Carnegie-Mellon-Berkeley (CMB) [3], and George Washington (GW) [4] groups.

All of these studies essentially agree on the existence and (most) properties of the 4-star states. For the 3-star and lower states, however, even a statement of existence is problematic. Many states claimed in the KH and CMB fits have not been found in recent GW analyses. This discrepancy clearly impacts the "missing resonance" problem, which has more quark model states predicted than observed. If many 3-star and lower rated states are not observed in πN scattering data (where they were first identified) then many more states are either "missing" or weakly coupled to the πN channel.

These problems have motivated a reexamination of the KH analysis [5] and further improvements to the ongoing GW studies. We have recently added data from the reaction $\pi N \to \eta N$, to better describe the πN S wave and the $N(1535)S_{11}$ resonance, which have a significant coupling to the ηN final state [6]. In the present study, we have extended the energy upper limit from 2.1 to 2.6 GeV, in the lab pion kinetic energy, to cover the resonance region more completely. This extended energy range will be carried over to our fits of pion photoproduction and electroproduction data, which are parametrized in terms of the πN scattering amplitudes. The extended energy range for photoproduction should allow us to fit all single-pion photoproduction data expected from the present generation of Jefferson Lab experiments.

A description of the coupled-channel analysis of πN elastic and ηN production data, constrained by dispersion relations, is given in Ref. [4] and will not be repeated here. In this report, we will concentrate on new features seen over our extended energy region and changes to the fit below 2.1 GeV. These are discussed in Sec. III. Changes to the database are described in Sec. II. We have mainly added data from 2.1 to 2.6 GeV but have also included new measurements at very low energies. Some of these require special attention. Finally, in Sec. IV, we summarize our results.

II. DATABASE

The first two decades (1957 through 1979) of experiments focused on the πN system and nonstrange baryon resonances produced a large amount of data below 2.6 GeV (9932 $\pi^+ p$, 9637 $\pi^- p$, and 1569 charge-exchange data). These data were used in the canonical KH [2] and CMB [3] analyses. In the present study, we have fitted 13344 $\pi^+ p$, 11967 $\pi^- p$, 2933 charge-exchange, and 257 η-production data. This increase is primarily due to a second generation of πN measurements (both unpolarized and polarized) carried out at high-intensity facilities such as LAMPF, TRIUMF, and PSI (former SIN). These more recent measurements generally have small statistical and systematic uncertainties and, therefore, have a significant influence on fits to the full database.

The evolution of our database is summarized in Table I. Over the course of five previous pion-nucleon analyses [4,7–10], our energy range was extended from 1.1 to 2.1 GeV in the lab pion kinetic energy. Here we have incorporated missed measurements below 2.1 GeV and the existing database to 2.6 GeV (but the η production database was not extended) using the Durham RAL Database [11].

In the following, we list recent (post 2003) additions below 2 GeV for elastic scattering, charge-exchange scattering, and η production. As in previous fits, not all of the available data have been used. Some data with very large χ^2 contributions have been excluded from our fits. Redundant data are also excluded. These include total elastic cross sections based on differential cross sections already contained in the database. Measurements of P with uncertainties of more than 0.2 are not included as they have little influence in our fits. However, all available data have been retained in the database (with the excluded data labeled as "flagged" [12]) so that comparisons can be made through our on-line facility [14]. Some of the data, listed as new, were available in unpublished form at the time of our previous analysis [4]. A complete description of the database and those data not included in our fits is available from the authors [14].

Most recent $\pi^{\pm}p$ measurements have been performed at low energies, TRIUMF being the main source. From this laboratory, we have added 274 $\pi^+ p$ and 271 $\pi^- p$ differential cross sections from 20 to 40 MeV. These data cover a broad angular range from 10° (including the Coulomb-nuclear interference region) to 170° [15] and have allowed us to extend

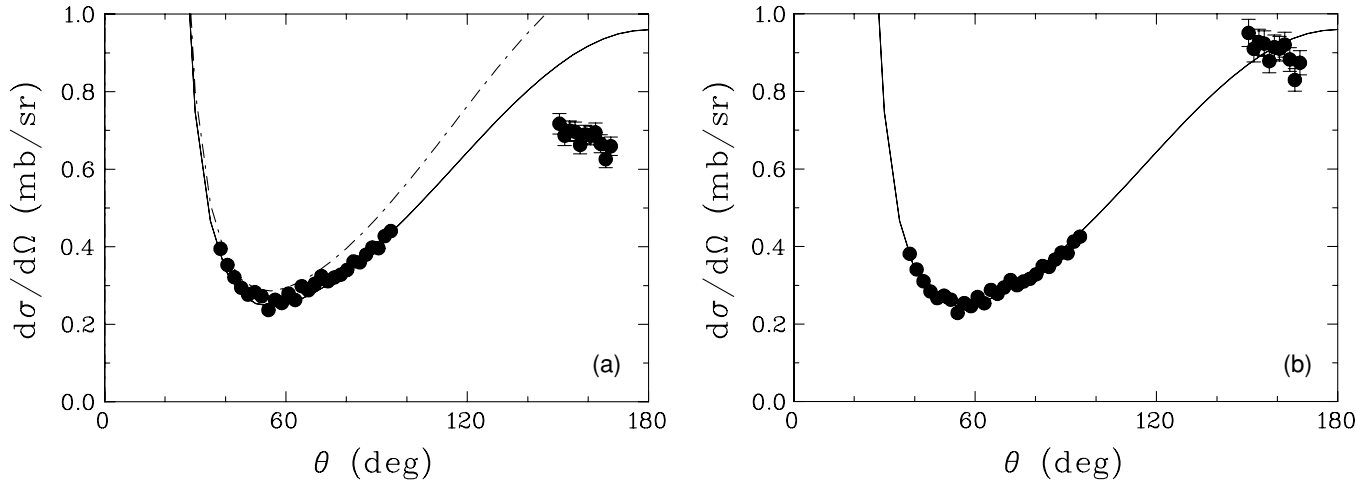

FIG. 1. Differential cross sections for $\pi^+ p$ elastic scattering at 26 MeV: (a) unnormalized and (b) normalized data. The Karlsruhe KA84 prediction [2] is plotted as a dot-dashed line. Data are taken from Ref. [15].

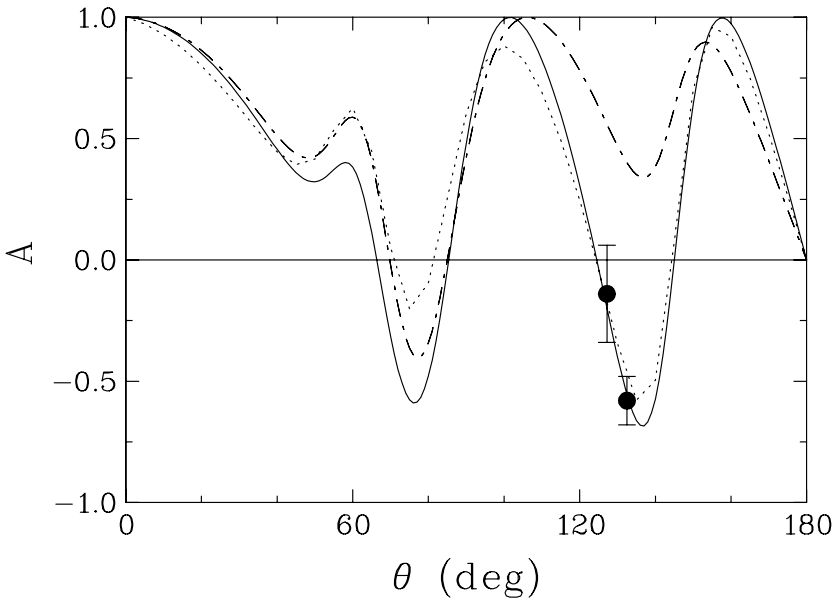

FIG. 2. Spin-rotation parameter A for $\pi^+ p$. The original KA84 solution [2] (dot-dashed line) is compared to a Barrelet-transformed solution [22] (dotted line) and our SP06 solution (solid line). Data are taken from Ref. [21].

TABLE I. Comparison of present (SP06) and previous (FA02 [4], SM95 [7], FA93 [8], SM90 [9], and FA84 [10]) energy-dependent partial-wave analyses of elastic $\pi^\pm p$, charge-exchange ($\pi^0 n$), and $\pi^- p \to \eta n$ (ηn) scattering data. For both SP06 and FA02 solutions, ηN data have been included to 800 MeV. The older Karlsruhe KA84 and KH80 results [2] are included for comparison. $N_{\rm prm}$ is the number of parameters ($I = 1/2$ and $3/2$) varied in the fit. SP06* gives the SP06 result evaluated over the energy range of our previous fits.

Solution	Range (MeV)	$\chi^2/\pi^+ p$	$\chi^2/\pi^- p$	$\chi^2/\pi^0 n$	$\chi^2/\eta n$	$N_{\rm prm}$
SP06	2600	27155/13344	22702/11967	6084/2933	626/257	93/81
KA84	2600	48394/13344	61845/11967	9410/2933		
KH80	2600	32468/13344	40634/11967	8005/2933		
SP06*	2100	22879/11842	18701/10561	4945/2640	626/257	93/81
FA02	2100	21735/10468	18932/9650	4136/1690	439/173	86/70
SM95	2100	23593/10197	18855/9421	4442/1625		94/80
FA93	2100	23552/10106	20747/9304	4834/1668		83/77
SM90	2100	24897/10031	24293/9344	10814/2132		76/68
FA84	1100	7416/3771	10658/4942	2062/717		64/57

TABLE II. Single-energy (binned) fits of combined elastic $\pi^{\pm}p$, charge-exchange, and $\pi^- p \to \eta n$ scattering data. $N_{\rm prm}$ gives the number of parameters varied in each single-energy fit and χ^2_E is given by the energy-dependent fit, SP06, over the same energy interval. $\delta\chi^2 = [\chi^2({\rm SP06}) - \chi^2({\rm SES})]$/data quantify the agreement between individual SES and SP06.

T_π (MeV)	Range (MeV)	$N_{\rm prm}$	χ^2/data	χ^2_E	$\delta\chi^2$
20	19–21	4	163/ 85	194	0.36
30	26–34	4	291/231	329	0.16
47	45–50	4	181/124	238	0.46
66	61–70	4	204/161	213	0.06
90	87–92	4	126/121	149	0.19
112	107–117	8	131/114	148	0.15
124	121–127	8	82/ 63	101	0.30
142	139–146	9	211/160	225	0.09
170	165–175	9	174/163	200	0.16
193	191–195	9	97/107	117	0.19
217	214–221	9	106/109	145	0.36
238	235–241	9	111/115	143	0.28
266	263–271	9	152/123	181	0.24
292	291–294	10	155/129	208	0.41
309	306–311	10	158/140	180	0.16
334	332–336	11	93/ 58	139	0.79
352	351–352	11	64/109	84	0.18
390	370–410	11	259/119	318	0.50
425	420–430	12	170/162	215	0.28
465	450–480	14	266/178	358	0.52
500	490–510	15	382/245	444	0.25
520	511–529	17	132/125	176	0.35
535	530–540	19	270/247	321	0.21
560	555–565	20	387/270	601	0.79
580	570–590	20	439/401	542	0.26
600	595–605	20	275/274	414	0.51
625	620–630	21	182/164	234	0.32
660	645–675	23	573/426	727	0.36
720	700–740	26	383/307	597	0.70
745	735–755	26	362/257	609	0.96
765	755–775	26	375/381	549	0.46
782	776–788	27	170/116	353	0.72
800	790–810	27	634/441	747	0.26
820	813–827	28	431/393	518	0.22
875	865–885	28	661/444	880	0.49
890	886–894	28	238/203	456	1.07
900	895–905	28	515/409	776	0.64
930	920–940	28	338/287	534	0.68
960	950–970	32	350/332	570	0.66
1000	985–1015	36	688/442	839	0.34
1030	1020–1040	38	533/400	661	0.32
1045	1040–1050	40	301/210	406	0.50
1075	1070–1080	40	220/217	402	0.84
1100	1095–1105	40	266/229	362	0.42
1150	1140–1160	42	665/446	863	0.44
1180	1165–1185	44	644/444	801	0.35
1210	1200–1220	44	299/274	378	0.29
1245	1230–1260	44	690/420	830	0.33
1320	1300–1340	46	824/567	1036	0.37
1370	1365–1375	46	456/286	668	0.74
1400	1385–1415	46	587/423	871	0.67
1460	1450–1470	50	878/562	1377	0.89
1480	1465–1495	50	626/409	861	0.57
1570	1555–1585	54	568/478	826	0.54
1595	1580–1610	55	507/405	755	0.61
1660	1645–1675	56	695/496	976	0.57
1720	1705–1735	58	391/286	511	0.42
1755	1740–1770	58	716/457	880	0.36
1840	1825–1855	58	423/323	741	0.98
1870	1860–1880	58	642/441	1005	0.82
1930	1915–1945	58	757/549	1021	0.48
1970	1960–1980	58	532/271	730	0.73
2025	2010–2040	58	397/339	714	0.94
2075	2050–2100	58	928/425	1270	0.80
2125	2100–2150	58	773/492	1366	1.21
2175	2150–2200	58	1025/486	1373	0.72
2225	2200–2250	58	915/513	1299	0.75
2275	2250–2300	58	473/271	704	0.85
2325	2300–2350	58	662/419	870	0.50
2375	2350–2400	58	602/388	950	0.90
2425	2400–2450	58	205/186	679	2.55
2475	2450–2500	58	192/136	372	1.32
2525	2500–2550	58	497/171	889	2.29
2575	2550–2600	58	385/139	911	3.78

our single-energy fits to very low energies (20 MeV) for the first time (see Table II).

The TRIUMF cross sections for $\pi^{\pm}$ elastic scattering were measured simultaneously over the full angular range using the CHAOS facility. At low energies, however, the forward (backward) cross sections are determined from measurements of the charged pion (proton). We mention this because the full angular range is difficult to fit with a single systematic uncertainty. The backward angle data disagree with both the KH predictions and predictions based on our FA02 solution. Including these data in our fit did not solve the problem, as can be seen in Fig. 1(a). To resolve the conflict among forward,

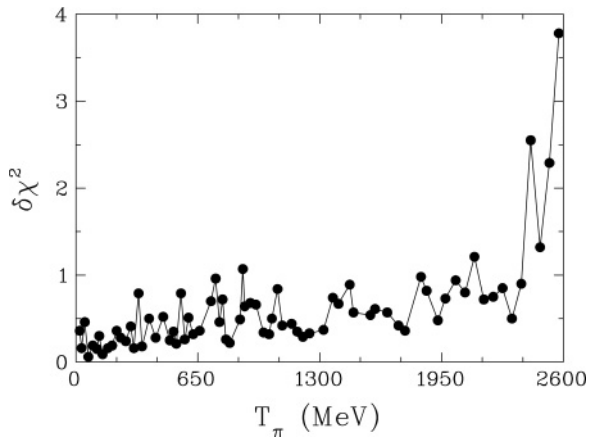

FIG. 3. Comparison of the SES and global SP06 fits via $\delta\chi^2 = [\chi^2({\rm SP06}) - \chi^2({\rm SES})]$/data presented in Table II.

TABLE III. Comparison of χ^2/data for normalized (Norm) and unnormalized (Unnorm) data used in the SP06 and FA02 [4] solutions. Karlsruhe KA84 and KH80 results [2] are included for comparison. Values for FA02 correspond to a 2.1-GeV energy limit. SP06, KH80, and KA84 are evaluated up to 2.6 GeV.

Reaction	SP06		FA02		KA84		KH80	
	Norm	Unnorm	Norm	Unnorm	Norm	Unnorm	Norm	Unnorm
$\pi^+ p \to \pi^+ p$	2.0	6.7	2.1	9.3	3.6	10.0	2.4	8.5
$\pi^- p \to \pi^- p$	1.9	6.2	2.0	7.1	5.2	13.0	3.4	10.2
$\pi^- p \to \pi^0 n$	2.1	4.5	2.4	9.5	3.2	7.8	2.7	5.9
$\pi^- p \to \eta n$	2.4	10.1	2.5	4.6				

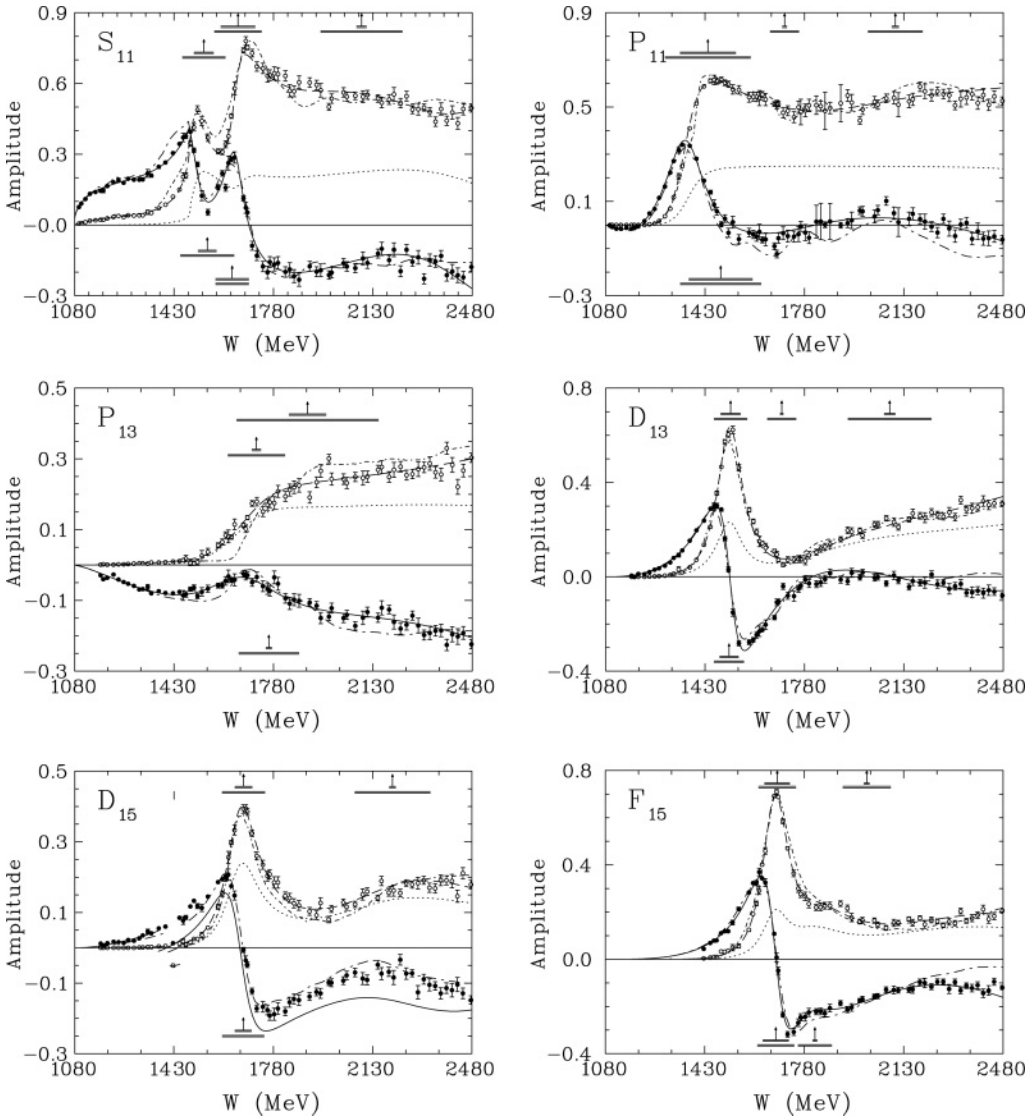

FIG. 4. Isospin 1/2 partial-wave amplitudes $J < 3$ ($L_{2I,2J}$) from $T_\pi = 0$ to 2.6 GeV. Solid (dashed) curves give the real (imaginary) parts of amplitudes corresponding to the SP06 solution. The real (imaginary) parts of single-energy solutions are plotted as filled (open) circles. The dotted curve gives the unitarity limit ($\mathrm{Im}T - T^*T$) from SP06. The Karlsruhe KA84 solution [2] is plotted with long dash-dotted (real part) and short dash-dotted (imaginary part) lines. All amplitudes are dimensionless. Vertical arrows indicate resonance W_R values and horizontal bars show full Γ and partial widths for $\Gamma_{\pi N}$. The lower BW resonance symbols are associated with the SP06 values of Table VI; upper symbols give RPP [1] values.

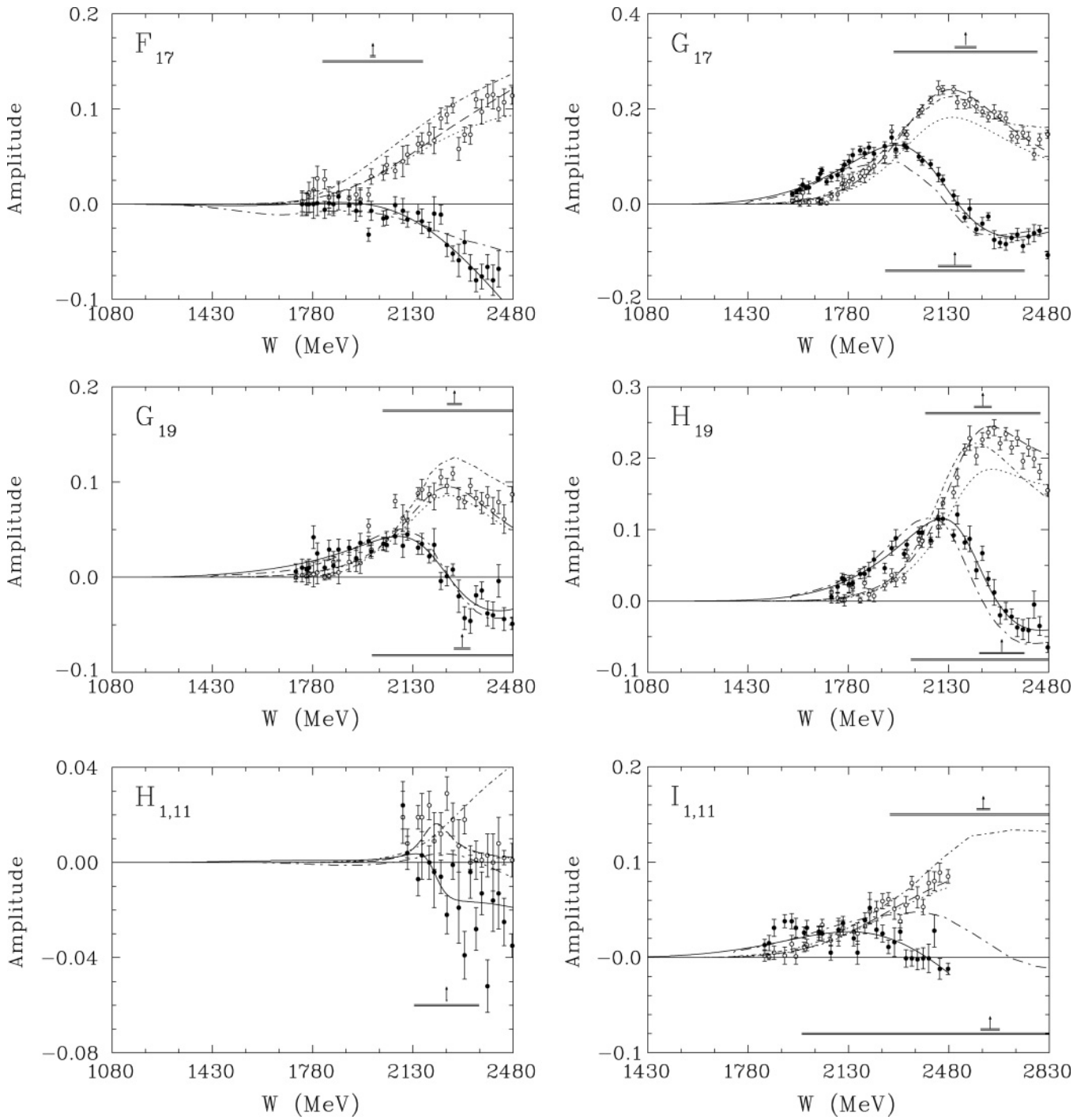

FIG. 5. Isospin 1/2 partial-wave amplitudes $J > 3$ ($L_{2I,2J}$) from $T_\pi = 0$ to 2.6 GeV. Notation as in Fig. 4.

medium, and backward scattering measurements, we divided the data into two or three pieces and treated them independently [Fig. 1(b)]. Clearly, the angular dependence at backward angles is not reproduced by SP06, nor was it reproduced by our single-energy fit. The reason for this conflict is unclear.

Further low-energy additions include 25 $\pi^+ p$ and 3 $\pi^- p$ A_y data between 50 and 130 MeV, at medium scattering angles, measured at PSI [16]. New total cross sections for charge-exchange measurements between 40 and 250 MeV came from PSI recently [17]. They have very little effect and seem quite well fitted by SP06 without any adjustment. Two BNL-AGS experiments from the Crystal Ball Collaboration have also been analyzed and added to our database. These include 648 charge-exchange data between 520 and 620 MeV [18] and 84 η-production data between 560 and 620 MeV [19]. The angular

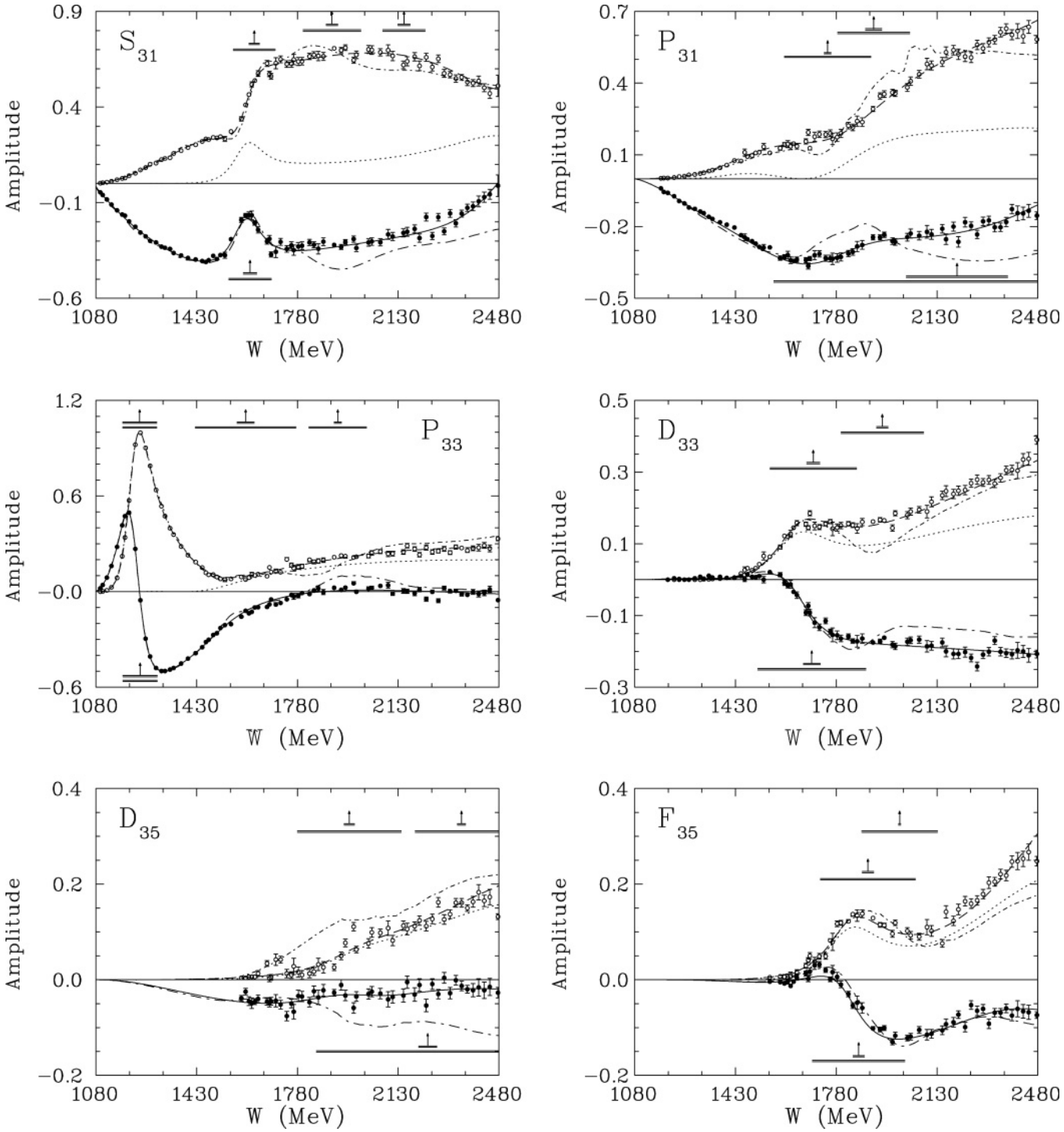

FIG. 6. Isospin 3/2 partial-wave amplitudes $J < 3$ ($L_{2I,2J}$) from $T_\pi = 0$ to 2.6 GeV. The lower BW resonances are associated with the SP06 values of Table VI; upper symbols give RPP [1] values. Notation as in Fig. 4.

coverage was 30° to 160° in both cases. Results based on the inclusion of these η-production data are given in Ref. [6].

Finally, ITEP–PNPI $\pi^- p$ experiments have provided three P and three A measurements at 1300 MeV in the backward direction [20]. Previous measurements of the $\pi^+ p$ spin-rotation parameter A, by the same collaboration [21], allowed us to resolve a discrepancy between the GW and the CMB/KH predictions (Fig. 2), using the method of Barrelet. These new measurements agree with predictions from our older FA02 and SM95 solutions.

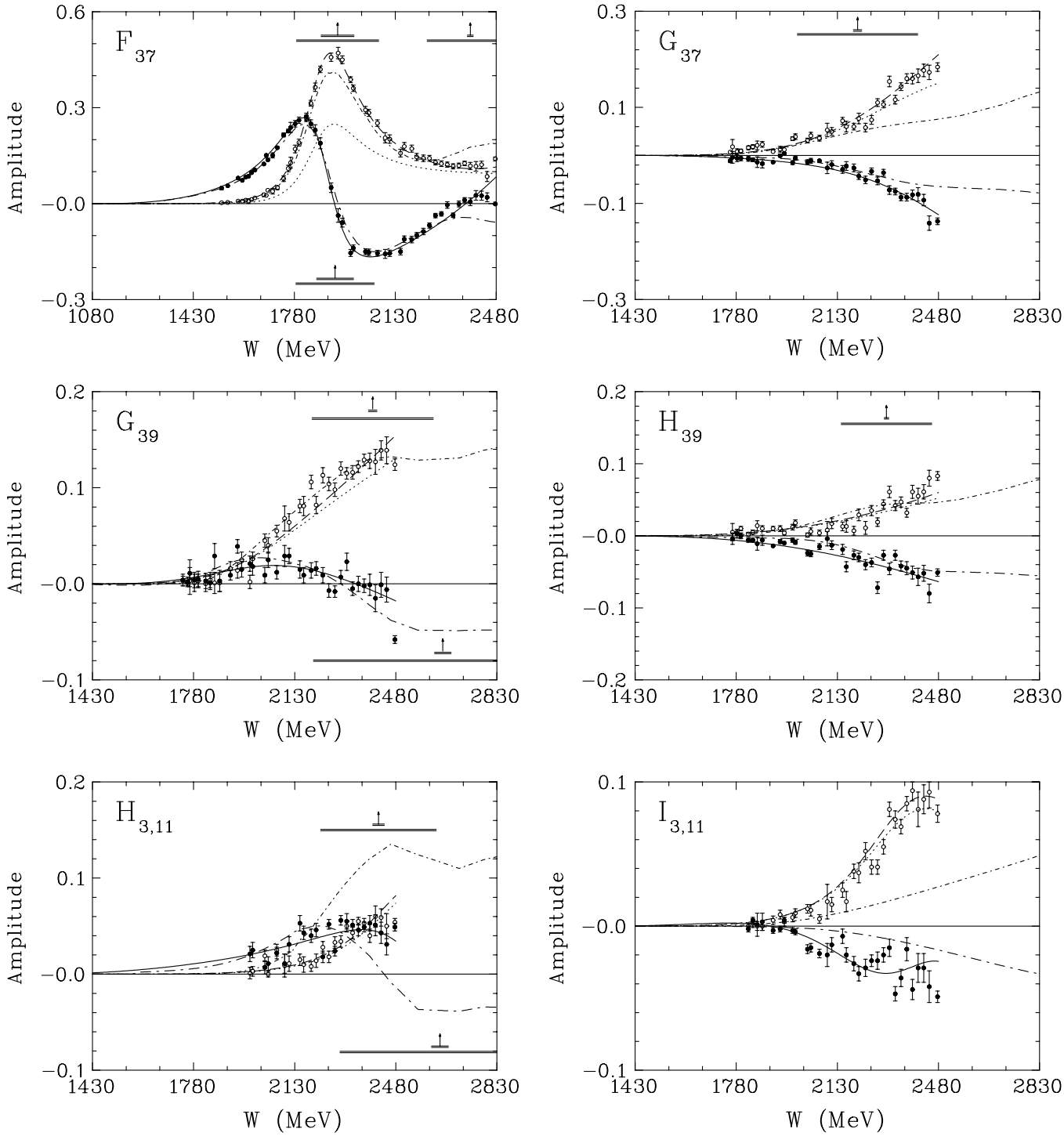

FIG. 7. Isospin 3/2 partial-wave amplitudes $J > 3$ ($L_{2I,2J}$) from $T_\pi = 0$ to 2.6 GeV. Notation as in Fig. 6.

III. RESULTS AND DISCUSSION

A. SP06 versus the FA02 and KH fits

The main result of this work is an energy-dependent solution (SP06), fitting data from threshold to 2.6 GeV, and a set of single-energy solutions (SES) ranging from 20 MeV to 2.575 GeV. Our present and previous energy-dependent solutions are compared in Table I. Results from the KH solutions are listed here as well. A comparison of SP06 and our previous solution FA02, up to the energy limit of FA02, shows that a fit to higher energies is possible without degrading the description of data below 2.1 GeV.

As in previous analyses, we have used the systematic uncertainty as an overall normalization factor for angular distributions. With each angular distribution, we associate the pair (X, ϵ_X): a normalization constant (X) and its uncertainty (ϵ_X).

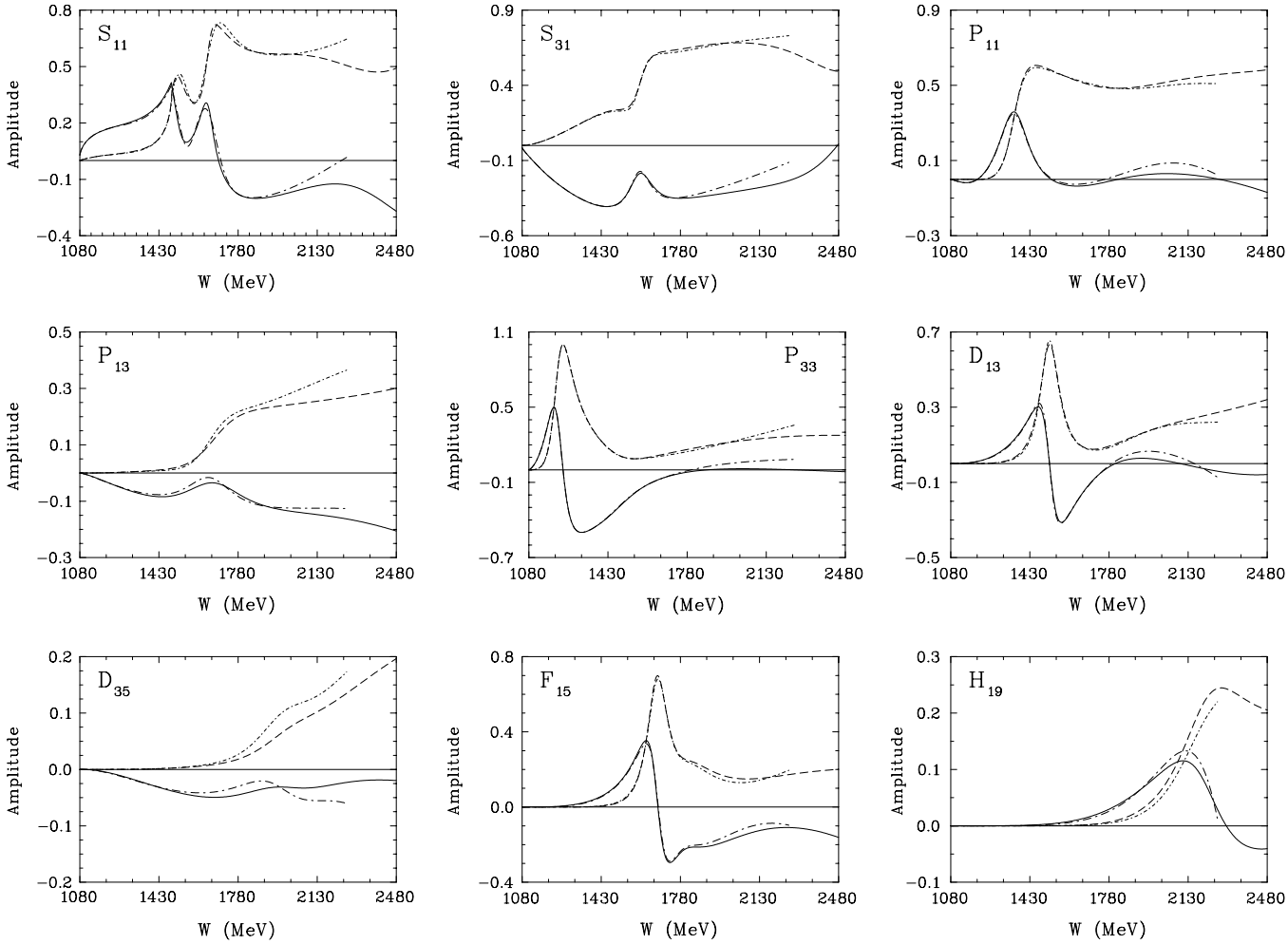

FIG. 8. Comparison of isospin 1/2 and 3/2 partial-wave amplitudes ($L_{2I,2J}$) from $T_\pi = 0$ to 2.6 GeV. Solid (dashed) curves give the real (imaginary) parts of the SP06 amplitudes. The FA02 solution (valid to 2.1 GeV) [4] is plotted with long dash-dotted (real part) and short dash-dotted (imaginary part) lines. All amplitudes are dimensionless.

The quantity ϵ_X is generally associated with the systematic uncertainty (if known.) The modified χ^2 function, to be minimized, is then given by

$$\chi^2 = \sum_i \left(\frac{X\theta_i - \theta_i^{\exp}}{\epsilon_i} \right)^2 + \left(\frac{X-1}{\epsilon_X} \right)^2, \qquad (1)$$

where the subscript i labels data points within the distribution, $\theta_i^{\exp}$ is an individual measurement, θ_i is the calculated value, and ϵ_i is the statistical uncertainty. For total cross sections and excitation data, we have combined statistical and systematic uncertainties in quadrature.

Renormalization freedom significantly improves our best-fit results, as shown in Table III. This renormalization procedure was also applied to the KH solutions. Here, however, only the normalization constants were searched to minimize χ^2 (since no adjustment of the partial waves was possible). In cases where the systematic uncertainty varies with angle, this procedure may be considered a first approximation. Clearly, this procedure can significantly improve the overall χ^2 attributed to a fit and has been applied in calculating the χ^2 values of Table I.

In Table II, we compare the energy-dependent and SES results over the energy bins used in each single-energy analysis. The quantity $\delta\chi^2$ computes $[\chi^2(\text{SP06}) - \chi^2(\text{SES})]$ divided by the number of data in each single-energy bin, providing a measure of the agreement between an individual SES and the global SP06 results (see Fig. 3). Also listed is the number of parameters varied in each SES. As was emphasized in Ref. [4], the SES are generated mainly to search for missing structures in the global fit.

Figures 4 through 7 compare the energy-dependent fits SP06 and KA84 [2] over the SP06 energy range (with KA84 valid to 10 GeV/c). The SP06 analysis has fitted waves up to $l = 8$, compared to $l = 7$ for FA02. Deviations from the KA84 results are largest in the isospin 3/2 amplitudes. One possible explanation is illustrated in Fig. 2, which compares the KA84 solution to a Barrelet-transformed version versus the double-polarization quantity A for $\pi^+ p$ ($I = 3/2$) scattering. This exercise and resulting changes to the KA84 isospin 3/2 amplitudes were discussed in Ref. [22] (see also the comments

in Ref. [23]). The agreement between SP06 and KA84 for $\pi^- p$ A data [20] is much closer, suggesting the absence of a Barrelet ambiguity in the isospin 1/2 amplitudes. Deviations from FA02 are visible mainly near the end point of the FA02 analysis. Some examples are given in Fig. 8.

B. Resonance parameter extraction

The resonance spectrum of our fit has been extracted in terms of poles and residues found by continuing into the complex energy plane. These are compiled in Tables IV and V. Zeros can be found in a similar manner and have been listed in a previous paper [4]. The location of a zero is not directly related to resonance properties, but the close proximity of zeros and poles may indicate cases where a simple Breit-Wigner parametrization is questionable.

TABLE IV. Pole positions from the solution SP06, our previous solution FA02 [4], and a range from the Particle Data Group [RPP] [1] (in square brackets). Real (W_R) and imaginary ($-2W_I$) parts are listed for isospin 1/2 baryon resonances. The second sheet pole is labeled by a †. Modulus and phase values are listed for the πN elastic pole residue.

Wave	W_R (MeV)	$-2W_I$ (MeV)	Modulus (MeV)	Phase (deg)	Ref.
S_{11}	1502	95	16	−16	SP06
	1526	130	33	+14	FA02
	[1490–1530]	[90–250]			RPP
S_{11}	1648	80	14	−69	SP06
	1653	182	69	−55	FA02
	[1640–1670]	[150–180]			RPP
P_{11}	1359	162	38	−98	SP06
	1357	160	36	−102	FA02
	[1350–1380]	[160–220]			RPP
$P_{11}^{\dagger}$	1388	165	86	−46	SP06
	1385	166	82	−51	FA02
					RPP
P_{13}	1666	355	25	−94	SP06
	1655	278	20	−88	FA02
	[1660–1690]	[115–275]			RPP
D_{13}	1515	113	38	−5	SP06
	1514	102	35	−6	FA02
	[1505–1515]	[105–120]			RPP
D_{15}	1657	139	27	−21	SP06
	1659	146	29	−22	FA02
	[1655–1665]	[125–150]			RPP
F_{15}	1674	115	42	−4	SP06
	1678	120	43	+1	FA02
	[1665–1680]	[110–135]			RPP
F_{15}	1807	109	60	−67	SP06
	1779	248	47	−61	FA02
					RPP
G_{17}	2070	520	72	−32	SP06
	2076	502	68	−32	FA02
	[2050–2100]	[400–520]			RPP
H_{19}	2199	372	33	−33	SP06
	2209	564	96	−71	FA02
	[2130–2200]	[400–560]			RPP
G_{19}	2217	431	21	−20	SP06
	2238	536	33	−25	FA02
	[2150–2250]	[350–550]			RPP
$H_{1,11}$	2203	133	1	−12	SP06
					FA02
					RPP

TABLE V. Pole positions for isospin 3/2 baryon resonances. Notation as in Table IV.

Wave	W_R (MeV)	$-2W_I$ (MeV)	Modulus (MeV)	Phase (deg)	Ref.
S_{31}	1595	135	15	−92	SP06
	1594	118	17	−104	FA02
	[1590–1610]	[115–120]			RPP
P_{31}	1771	479	45	+172	SP06
	1748	524	48	+158	FA02
	[1830–1880]	[200–500]			RPP
P_{33}	1211	99	52	−47	SP06
	1210	100	53	−47	FA02
	[1209–1211]	[98–102]			RPP
P_{33}	1457	400	44	+147	SP06
					FA02[a]
	[1500–1700]	[200–400]			RPP
D_{33}	1632	253	18	−40	SP06
	1617	226	16	−47	FA02
	[1620–1680]	[160–240]			RPP
D_{35}	2001	387	7	−12	SP06
	1966	364	16	−21	FA02
	[1840–1960]	[175–360]			RPP
F_{35}	1819	247	15	−30	SP06
	1825	270	16	−25	FA02
	[1825–1835]	[265–300]			RPP
F_{37}	1876	227	53	−31	SP06
	1874	236	57	−34	FA02
	[1870–1890]	[220–260]			RPP
G_{39}	1983	878	24	−139	SP06
					FA02
					RPP[b]
$H_{3,11}$	2529	621	33	−45	SP06
					FA02
	[2260–2400]	[350–750]			RPP

[a] A second P_{33} state was not reported in FA02.
[b] No RPP average given.

The more commonly used, and more model-dependent, Breit-Wigner parameters for resonances are listed in Tables VI and VII. Here, in the FA02 and SM95 fits, a unitary Breit-Wigner plus background form was assumed for the resonant partial wave. Data within an energy bin were then fitted using this representation. The remaining waves were fixed to values found in the full global analysis. Energy ranges over which fits were performed and χ^2 comparisons are given in Tables VIII and IX. This method is more directly linked to data than a fit to the SES. However, the resulting parameter uncertainties tend to be small, reflecting the statistical error but not the (possibly large) systematic error associated with a separation of resonance and background contributions. The pole and Breit-Wigner representations are compared in Fig. 9.

The onset of resonant behavior, seen in the FA02 G_{17}, G_{19}, and H_{19} partial waves, is fully developed in SP06, the extension

TABLE VI. Resonance couplings from a Breit-Wigner fit to the SP06 solution, our previous solution FA02 [4], and a range from the [RPP] [1] (in square brackets). Masses W_R, widths Γ, and partial width $\Gamma_{\pi N}/\Gamma$ are listed for isospin 1/2 baryon resonances. $\Gamma_{\pi N}/\Gamma$ for $N(1650)S_{11}$ is not varied in the BW fit.

Resonance	W_R (MeV)	Γ (MeV)	$\Gamma_{\pi N}/\Gamma$	Ref.
$N(1440)P_{11}$	1485.0 ± 1.2	284 ± 18	0.787±0.016	SP06
	1468.0 ± 4.5	360 ± 26	0.750±0.024	FA02
	[1420–1470]	[200–450]	[0.55–0.75]	RPP
$N(1520)D_{13}$	1514.5 ± 0.2	103.6 ± 0.4	0.632±0.001	SP06
	1516.3 ± 0.8	98.6 ± 2.6	0.640±0.005	FA02
	[1515–1525]	[100–125]	[0.55–0.65]	RPP
$N(1535)S_{11}$	1547.0 ± 0.7	188.4 ± 3.8	0.355±0.002	SP06
	1546.7 ± 2.2	178.0 ± 11.6	0.360±0.009	FA02
	[1525–1545]	[125–175]	[0.35–0.55]	RPP
$N(1650)S_{11}$	1634.7 ± 1.1	115.4 ± 2.8	1.000	SP06
	1651.2 ± 4.7	130.6 ± 7.0	1.000	FA02
	[1645–1670]	[145–185]	[0.60–0.95]	RPP
$N(1675)D_{15}$	1674.1 ± 0.2	146.5 ± 1.0	0.393±0.001	SP06
	1676.2 ± 0.6	151.8 ± 3.0	0.400±0.002	FA02
	[1670–1680]	[130–165]	[0.35–0.45]	RPP
$N(1680)F_{15}$	1680.1 ± 0.2	128.0 ± 1.1	0.701±0.001	SP06
	1683.2 ± 0.7	134.4 ± 3.8	0.670±0.004	FA02
	[1680–1690]	[120–140]	[0.65–0.70]	RPP
$N(1720)P_{13}$	1763.8 ± 4.6	210 ± 22	0.094±0.005	SP06
	1749.6 ± 4.5	256 ± 22	0.190±0.004	FA02
	[1700–1750]	[150–300]	[0.10–0.20]	RPP
$N(2000)F_{15}$	1817.7	117.6	0.127	SP06
				FA02
	[2000]			RPP
$N(2190)G_{17}$	2152.4 ± 1.4	484 ± 13	0.238±0.001	SP06
	2192.1 ± 8.7	726 ± 62	0.230±0.002	FA02
	[2100–2200]	[300–700]	[0.10–0.20]	RPP
$N(2220)H_{19}$	2316.3 ± 2.9	633 ± 17	0.246±0.001	SP06
	2270 ± 11	366 ± 42	0.200±0.006	FA02
	[2200–2300]	[350–500]	[0.10–0.20]	RPP
$N(2245)H_{1,11}$	2247.2 ± 6.2	225 ± 23	0.014±0.001	SP06
				FA02
				RPP
$N(2250)G_{19}$	2302 ± 6	628 ± 28	0.089±0.001	SP06
	2376 ± 43	924 ± 178	0.110±0.004	FA02
	[2200–2350]	[230–800]	[0.05–0.15]	RPP
$N(2600)I_{1,11}$	2623 ± 197	1311 ± 996	0.050±0.018	SP06
				FA02
	[2550–2750]	[500–800]	[0.05–0.10]	RPP

by 500 MeV in T_π corresponding to a 200-MeV increase in center-of-mass energy. We can now also see resonant behavior in the G_{39}, $H_{3,11}$, and $I_{1,11}$ waves. A possible resonance is seen in $H_{1,11}$, though the SES scatter is large and the amplitude is small in magnitude.

We have tried to associate each state with its corresponding PDG designation. In some cases, this resulted in a resonance mass far from that of a "named" resonance. One such case is the $N(2000)F_{15}$. We find evidence for a second F_{15} state closer to 1800 MeV. The KH analysis also finds a mass near 1880 MeV, which suggests a name change for this 2-star state may be in order. In SP06, this second F_{15} resonance was found by scanning each partial wave for small structures.

TABLE VII. Parameters for isospin 3/2 baryon resonances. Notation as in Table VI. $\Gamma_{\pi N}/\Gamma$ for $\Delta(1232)P_{33}$ is not varied in the BW fit.

Resonance	W_R (MeV)	Γ (MeV)	$\Gamma_{\pi N}/\Gamma$	Ref.
$\Delta(1232)P_{33}$	1233.4 ± 0.4	118.7 ± 0.6	1.000	SP06
	1232.9 ± 1.2	118.0 ± 2.2	1.000	FA02
	[1231–1233]	[116–120]	[1.0]	RPP
$\Delta(1620)S_{31}$	1615.2 ± 0.4	146.9 ± 1.9	0.315±0.001	SP06
	1614.1 ± 1.1	141.0 ± 6.0	0.310±0.004	FA02
	[1600–1660]	[135–150]	[0.20−0.30]	RPP
$\Delta(1700)D_{33}$	1695.0 ± 1.3	375.5 ± 7.0	0.156±0.001	SP06
	1687.9 ± 2.5	364.8 ± 16.6	0.150±0.001	FA02
	[1670–1750]	[200–400]	[0.10−0.20]	RPP
$\Delta(1905)F_{35}$	1857.8 ± 1.6	320.6 ± 8.6	0.122±0.001	SP06
	1855.7 ± 4.2	334 ± 22	0.120±0.002	FA02
	[1865–1915]	[270–400]	[0.09−0.15]	RPP
$\Delta(1910)P_{31}$	2067.9 ± 1.7	543.0 ± 10.1	0.239±0.001	SP06
	2333 ± 36	1128 ± 238	0.390±0.019	FA02
	[1870–1920]	[190–270]	[0.15−0.30]	RPP
$\Delta(1930)D_{35}$	2233 ± 53	773 ± 187	0.081±0.012	SP06
	2046 ± 45	402 ± 198	0.040±0.014	FA02
	[1900–2020]	[220–500]	[0.05−0.15]	RPP
$\Delta(1950)F_{37}$	1921.3 ± 0.2	271.0 ± 1.1	0.471±0.001	SP06
	1923.3 ± 0.5	278.2 ± 3.0	0.480±0.002	FA02
	[1915–1950]	[235–335]	[0.35−0.45]	RPP
$\Delta(2400)G_{39}$	2643 ± 141	895 ± 432	0.064±0.022	SP06
				FA02
	[2400]			RPP
$\Delta(2420)H_{3,11}$	2633 ± 29	692 ± 47	0.085±0.008	SP06
				FA02
	[2300–2500]	[300–500]	[0.05−0.15]	RPP

TABLE VIII. Comparison of SP06 and BW plus background representations for isospin 1/2 baryon resonance fits (see text and associated Table VI). "Data" refer to the number of scattering data between $W_{\min}$ and $W_{\max}$.

Resonance	$W_{\min}$ (MeV)	$W_{\max}$ (MeV)	BW fit χ^2	SP06 χ^2	Data
$N(1440)P_{11}$	1350	1550	5437	5377	3104
$N(1520)D_{13}$	1480	1560	3350	3399	2068
$N(1535)S_{11}$	1490	1590	3451	3481	2195
$N(1650)S_{11}$	1620	1770	8658	8558	4678
$N(1675)D_{15}$	1610	1730	7072	7093	3932
$N(1680)F_{15}$	1620	1730	6326	6317	3443
$N(1720)P_{13}$	1620	1820	10701	10743	5837
$N(2190)G_{17}$	2050	2250	10414	10549	4908
$N(2220)H_{19}$	2150	2350	11649	11690	4660
$N(2245)H_{1,11}$	2050	2380	17451	17508	7573
$N(2250)G_{19}$	2050	2350	16073	16095	6895
$N(2600)I_{1,11}$	2070	2460	19554	19414	7590

TABLE IX. Comparison of SP06 and BW plus background representations for isospin 3/2 baryon resonance fits (see text and associated Table VII).

Resonance	$W_{\min}$ (MeV)	$W_{\max}$ (MeV)	BW fit χ^2	SP06 χ^2	Data
$\Delta(1232)P_{33}$	1180	1270	1283	1278	1016
$\Delta(1620)S_{31}$	1570	1680	4696	4715	2705
$\Delta(1700)D_{33}$	1550	1750	9959	9992	5490
$\Delta(1905)F_{35}$	1770	1920	7545	7567	4039
$\Delta(1910)P_{31}$	1650	2150	26540	25363	13258
$\Delta(1930)D_{35}$	1770	2100	16241	16176	8442
$\Delta(1950)F_{37}$	1800	2000	10842	10890	5437
$\Delta(2400)G_{39}$	2140	2460	16855	16626	6134
$\Delta(2420)H_{3,11}$	2150	2460	16149	16138	5970

Its resonance parameters have been determined through a fit to the full database and are quoted without errors.

The $\Delta(1910)P_{31}$ is also problematic. We find only a single P_{31} state, with a pole position more in line with the (1-star) $\Delta(1750)P_{31}$ than the (4-star) $\Delta(1910)P_{31}$. As can be seen in Fig. 6, the P_{31} resonance signature is particularly subtle for a 4-star state. Small changes in the KH and CMB amplitudes, owing to the Barrelet ambiguity, could explain this mass shift. Our Breit-Wigner fits to this structure yielded spurious results, with a mass several hundred MeV above the pole position and a width exceeding 1 GeV, if data were fitted around the assumed 4-star state mass. More reasonable values were obtained when the fitted energy range was expanded. This fit to a Breit-Wigner form is questionable for states with poles so far from the physical axis (see Fig. 9).

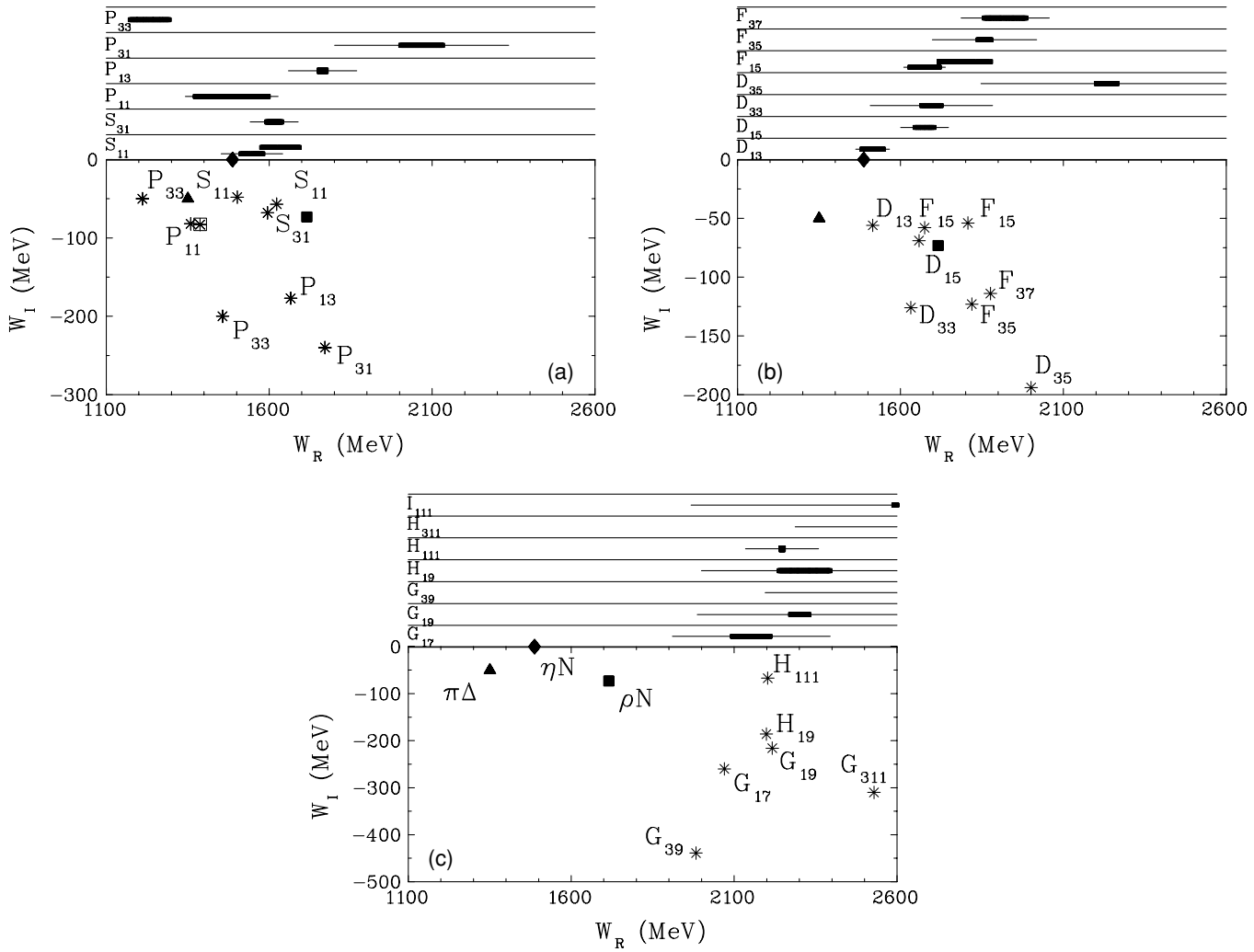

FIG. 9. Comparison of complex plane (bottom panel) and Breit-Wigner (top panel) parameters for resonances found in the SP06 solution. Plotted are the result for (a) S- and P-wave resonances, (b) D- and F-wave resonances, and (c) G-, H, and I-wave resonances. Complex plane poles are shown as stars (with the boxed star denoting a second-sheet pole). W_R and W_I give real and imaginary parts of the center-of-mass energy. The full (πN partial) widths are denoted by thin (thick) bars for each resonance. The branch point for $\pi\Delta(1232)$, 1350 - i50 MeV, is represented as a solid triangle. The branch points for ηN, 1487 -i0 MeV, and ρN, 1715 - i73 MeV, thresholds are shown as a solid diamond and solid square, respectively.

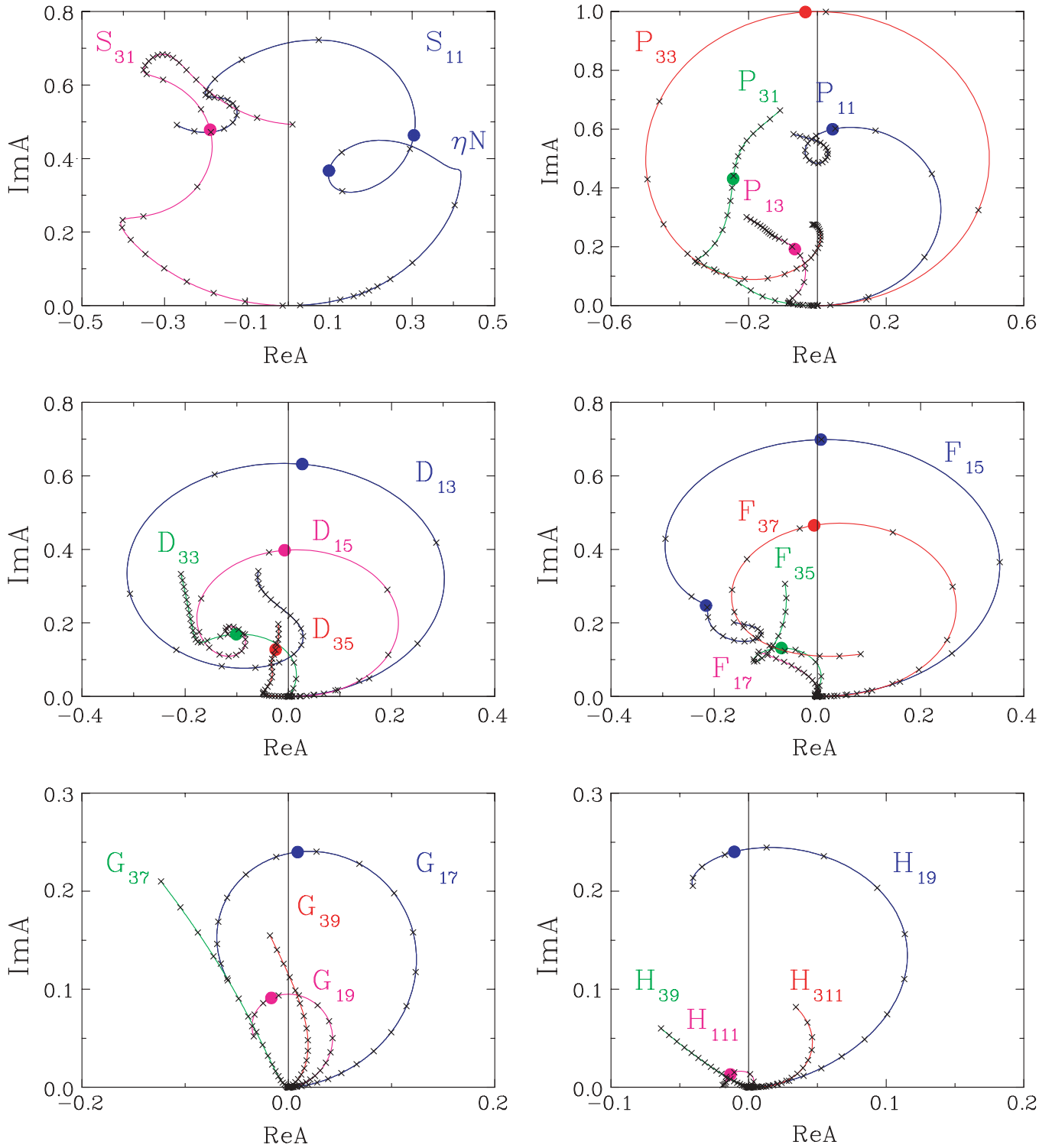

FIG. 10. (Color) Argand plots for partial-wave amplitudes from threshold (1080 MeV) to $W = 2.5$ GeV. Crosses indicate 50-MeV steps in W. Solid circles correspond to BW W_R determination presented in Tables VI and VII.

The P_{11} partial wave of KA84 and the SES associated with SP06 agree reasonably well over the full range of SP06. However, this does not lead to agreement on the resonance content. The prominent $N(1440)P_{11}$ resonance is clearly evident in both analyses, but it occurs very near the $\pi\Delta$ threshold, making a Breit-Wigner fit questionable [23]. Above this energy, the P_{11} partial wave wraps around the center of the Argand diagram (Fig. 10). As a result, small changes in the amplitude can produce large changes in the phase, though these changes have little influence on the data fit. States above

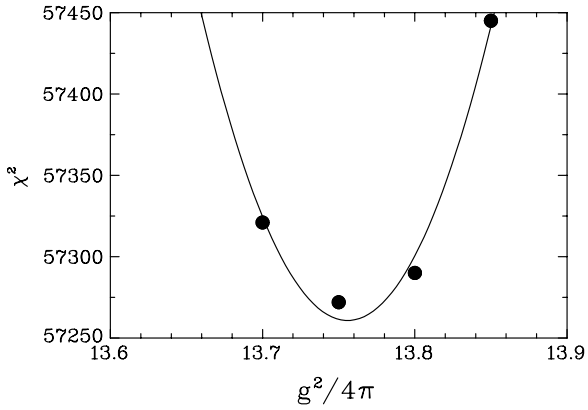

FIG. 11. Best-fit χ^2 as a function of the coupling constant $g^2/4\pi$, where all other parameters were fixed to their optimal (best-fit) values. The solid curve gives the best fit of χ^2 vs $g^2/4\pi$ assuming $\chi^2 = a + (\frac{g^2/4\pi - b}{c})^2$, where a, b, and c are free parameters.

the $N(1440)P_{11}$ should be established in reactions where they are more clearly required.

IV. SUMMARY AND CONCLUSIONS

We have fitted the existing πN elastic scattering and charge-exchange database to 2.6 GeV (with ηN data included to 800 MeV), employing a complete set of dispersion relation constraints, up to $T_\pi = 1$ GeV and $t = -0.4(\mathrm{GeV}/c)^2$. This extension in T_π has allowed us to search an addition 200 MeV of the resonance region (in center-of-mass energy).

Some resonance structures, at the limit of our FA02 analysis, are now better defined, whereas new structures have appeared in the G, H, and I waves. Both the SP06 and KH solutions are reasonably well within the spread of the isospin 1/2 SES (as shown in Figs. 4 and 5). However, the KH solutions are less smooth, suggesting the existence of additional resonances weakly coupled to the πN channel. In our opinion, such states should be established in reactions where they couple more strongly; the πN database can be fitted without these additional resonances. A comparison of SP06 and KH partial waves with isospin 3/2 is more interesting. The P_{31}, D_{33}, and D_{35} waves show large deviations, some of which have been qualitatively explained in Ref. [22]. In other isospin 3/2 waves there is better agreement. For example, the 2-star $\Delta(2400)G_{39}$ appears at the upper end of our analysis, with a mass, width, and elasticity in reasonable agreement with the KH values.

Other quantities of interest, such as the scattering lengths, the πN coupling constant, and the sigma term, are consistent with values obtained in the FA02 fit. In Fig. 11 we show a quadratic fit to χ^2 values from solutions with $g^2/4\pi$ ranging from 13.70 to 13.85, yielding the value $g^2/4\pi = 13.76 \pm 0.01$, in agreement with the FA02 result. Finally, we note that the sigma term was extracted from our FA02 solution, using interior dispersion relations, in Ref. [24]. We find that this quantity has changed by less than 2 MeV between FA02 and SP06.

ACKNOWLEDGMENTS

The authors express their gratitude to I. Alekseev, B. Johannes, R. Meier, S. Prakhov, G. R. Smith, A. Starostin, D. Svirida, and G. Wagner for providing experimental data prior to publication or for clarification of information already published. This work was supported in part by the U.S. Department of Energy under Grant No. DE-FG02-99ER41110. The authors (R. A., I. S., and R. W.) acknowledge partial support from Jefferson Lab and the Southeastern Universities Research Association under DOE Contract No. DE-AC05-84ER40150.

[1] W.-M. Yao *et al.*, Review of Particle Physics, J. Phys. G **33**, 1 (2006).

[2] G. Höhler, *Pion-Nucleon Scattering*, Landoldt-Börnstein Vol. **I/9b2**, edited by H. Schopper (Springer-Verlag, Berlin, 1983); R. Koch, Z. Phys. C **29**, 597 (1985); R. Koch (private communication). We have used the Karlsruhe solution KA84, generated through a FORTRAN subroutine supplied by R. Koch.

[3] R. E. Cutkosky, C. P. Forsyth, R. E. Hendrick, and R. L. Kelly, Phys. Rev. D **20**, 2839 (1979); R. E. Cutkosky, in *Proceedings of the 4th Conference on Baryon Resonances, Toronto, 1980*, edited by N. Isgur (World Scientific, Singapore, 1981), p. 19.

[4] R. A. Arndt, W. J. Briscoe, I. I. Strakovsky, R. L. Workman, and M. M. Pavan, Phys. Rev. C **69**, 035213 (2004).

[5] P. Piirola, E. Pietarinen, and M. E. Sainio, πN Newslett. **16**, 121 (2002).

[6] R. A. Arndt, W. J. Briscoe, T. W. Morrison, I. I. Strakovsky, R. L. Workman, and A. B. Gridnev, Phys. Rev. C **72**, 045202 (2005).

[7] R. A. Arndt, I. I. Strakovsky, R. L. Workman, and M. M. Pavan, Phys. Rev. C **52**, 2120 (1995).

[8] R. A. Arndt, R. L. Workman, and M. M. Pavan, Phys. Rev. C **49**, 2729 (1994).

[9] R. A. Arndt, L. Zhujun, L. D. Roper, R. L. Workman, and J. M. Ford, Phys. Rev. D **43**, 2131 (1991).

[10] R. A. Arndt, J. M. Ford, and L. D. Roper, Phys. Rev. D **32**, 1085 (1985).

[11] HEPDATA, The Durham RAL Database compiled by the Durham Database Group (UK) with help from the COMPAS group (Russia); http://www.slac.stanford.edu/spires/hepdata/reac.html.

[12] The 1-, 2-, and 3-star rating of data is described in Ref. [9]. Only 2- and 3-star data are included in the analyses. Unrated data are included unless they have been "flagged" for deletion from analyses. It should be noted that these flagged data are still retained in our database. We have followed this recipe since 1990 [13].

[13] Historically, B. M. K. Nefkens, W. J. Briscoe, M. M. Sadler, R. A. Arndt, and G. Höhler analyzed and classified all πN measurements completed before 1983. 0-, 1-, 2-, and 3-star ratings were assigned to the πN database entries. This star rating system was described at Few Body'83 and the 1st πN International Workshop by B. M. K. Nefkens, in *Few Body Problems in Physics (Contr. Papers) (Proceedings of 10th International Conference on Few Body Problems in Physics,*

Karlsruhe, Germany, 1983), edited by B. Zeitnitz (1984), p. 137; Nucl. Phys. **A416**, 193 (1984); and *Proceedings of the First Workshop on πN scattering, Karlsruhe, Germany, Aug. 1984*, edited by G. Höhler.

[14] The full database and numerous PWAs can be accessed via an ssh call to the SAID facility gwdac.phys.gwu.edu, with userid: said (no password), or a link to the website http://gwdac.phys.gwu.edu.

[15] H. Denz *et al.* (CHAOS Collaboration), Phys. Lett. **B633**, 209 (2006).

[16] R. Meier *et al*., Phys. Lett. **B588**, 155 (2004).

[17] J. Breitschopf *et al*., Phys. Lett. **B639** 424 (2006).

[18] A. Starostin *et al*. (Crystal Ball Collaboration), Phys. Rev. C **72**, 015205 (2005).

[19] S. Prakhov *et al*. (Crystal Ball Collaboration), Phys. Rev. C **72**, 015203 (2005).

[20] I. G. Alekseev *et al*., Eur. Phys. J. C **45**, 383 (2005).

[21] I. G. Alekseev *et al*., Phys. Lett. **B351**, 585 (1995).

[22] I. G. Alekseev, V. P. Kanavets, B. V. Morozov, D. N. Svirida, S. P. Kruglov, A. A. Kulbardis, V. V. Sumachev, R. A. Arndt, I. I. Strakovsky, and R. L. Workman, Phys. Rev. C **55**, 2049 (1997).

[23] G. Höhler and R. Workman in Ref. [1].

[24] G. E. Hite, W. B. Kaufmann, and R. J. Jacob, Phys. Rev. C **71**, 065201 (2005).